# Time-lapse crosswell seismic and VSP monitoring of injected $CO_2$ in a brine aquifer

Thomas M Daley*, Larry R. Myer, J.E. Peterson, E.L. Majer, G.M. Hoversten

all at Lawrence Berkeley National Laboratory, 1 Cyclotron Rd., Berkeley, Ca., 94720, USA

*tmdaley@lbl.gov

(Submitted to Environmental Geology, May 2006, revised Nov 2006)

Keywords: $CO_2$, sequestration, VSP, crosswell, seismic

## Abstract

Seismic surveys successfully imaged a small scale $CO_2$ injection (1600 tons) conducted in a brine aquifer of the Frio Formation near Houston, Texas. These time-lapse bore-hole seismic surveys, crosswell and vertical seismic profile (VSP), were acquired to monitor the $CO_2$ distribution using two boreholes (the new injection well and a pre-existing well used for monitoring) which are 30 m apart at a depth of 1500 m. The crosswell survey provided a high-resolution image of the $CO_2$ distribution between the wells via tomographic imaging of the P-wave velocity decrease (up to 500 m/s). The simultaneously acquired S-wave tomography showed little change in S-wave velocity, as expected for fluid substitution. A rock physics model was used to estimate $CO_2$ saturations of 10-20% from the P-wave velocity change. The VSP survey resolved a large (~70%) change in reflection amplitude for the Frio horizon. This $CO_2$ induced reflection amplitude change allowed estimation of the $CO_2$ extent beyond the monitor well and on

3 azimuths. The VSP result is compared with numerical modeling of $CO_2$ saturations and is seismically modeled using the velocity change estimated in the crosswell survey.

## Introduction

The geologic storage of $CO_2$ emitted from fixed sources, such as coal or gas power plants, is currently considered one of the prime technologies for short term (~ 50 year) mitigation of greenhouse gas emissions (Pacala and Socolow, 2004). Saline aquifers are generally considered a prime candidate for large scale storage. Initial studies have shown that time-lapse borehole and surface seismic surveys can be used to estimated the location of injected $CO_2$ in brine aquifers as well as in oil and gas reservoirs (Arts et al. 2002; Hoversten et al. 2003; Gritto et al. 2004; Xue et al. 2005). Monitoring of injected $CO_2$ will likely be a necessary component of any long term storage program. Therefore, understanding the seismic response of saline aquifers to injected $CO_2$ is an important goal.

As part of a U.S. Department of Energy (DOE) funded project on geologic sequestration of $CO_2$, we acquired borehole seismic surveys before and after injection of about 1600 tons of $CO_2$ into a saline aquifer. These time-lapse surveys consisted of crosswell and vertical seismic profile (VSP) experiments. These experiments were part of an integrated suite of scientific studies with many contributing institutions including the Texas Bureau of Economic Geology who performed the site selection process (Hovorka et al. 2006).

The VSP and crosswell are intermediate scale (1 - 100's m) geophysical surveys providing information in-between the large scale of surface seismic (km's) and the smaller scale of well logs and core measurements (mm to m). As such, they are useful tools for monitoring small scale injections and for understanding larger scale surface measurements. A summary of the VSP method and its uses is given in Balch and Lee (1984) and the crosswell method is described in Hardage (2000).

VSP and crosswell use different acquisition geometries, have different capabilities and are typically used for different goals. Figure 1a shows the VSP geometry has a surface source and borehole sensors recording direct and reflected energy. VSP data typically has higher resolution (about 10 - 30 m) than surface seismic (30 - 100 m) because the sensors are below the near surface, which is highly attenuative. Since VSP allows measurement of upgoing (reflected) and downgoing (direct) waves within the borehole depth range, it improves the tie of surface seismic to borehole measurements. The upgoing waves are those reflected from interfaces and correspond to the reflections imaged with surface seismic. Figure 1b shows the crosswell geometry, which has borehole sources and borehole sensors. The crosswell survey has higher resolution (about 1-5 m) because the subsurface source allows higher frequency propagation over (typically) shorter distances than surface source data. However the crosswell is limited to the interwell volume while the VSP can potentially image on any azimuth. Crosswell acquisition allows tomographic imaging of seismic velocity between the boreholes.

64 Crosswell seismic methods have been successfully applied to CO2 injection monitoring,
65 initially as part of enhanced oil recovery (EOR) (e.g. Harris et al.1995; Lazaratos and
66 Marion 1997; Gritto et al. 2004) and more recently as part of a sequestration pilot test
67 (Xue et al. 2005; Spetzler et al. 2006). These studies were successful in detecting
68 changes in seismic velocity caused by $CO_2$ injection into reservoirs. In the case of oil
69 reservoirs the interpretation can be more difficult because of multi phase fluids (e.g.
70 methane, brine, oil and $CO_2$, as described in Hoversten et al. 2003). In sequestration
71 pilots, the $CO_2$ is typically injected into brine aquifers (Arts et al. 2002; Xue et al. 2005).
72 Xue et al. (2005) found a velocity reduction of about 3% from crosswell tomography and
73 a reduction of up to 23% at the well bore via sonic logging. Arts et al. (2002) present
74 surface seismic monitoring results that show reflection amplitude change in the CO2
75 injection volume. The VSP method is useful for interpreting surface seismic and was
76 used in this way at the Weyburn field $CO_2$ EOR project (Majer et al. 2006).

77 The goals of the crosswell survey were to spatially map the $CO_2$ between the wells us-
78 ing P- and S-wave velocity tomographic imaging, and to use these properties to esti-
79 mate the $CO_2$ saturation between the wells. The goals of the VSP were to spatially map
80 the $CO_2$ beyond the well pair and to image nearby structures such as faults. The time-
81 lapse VSP and crosswell surveys were acquired together, with pre-injection surveys in
82 July 2004 and post-injection surveys in late November 2004, about 1.5 months after the
83 $CO_2$ injection.

In the following sections we will describe the geologic background, the data acquisition and analysis, interpretation of the results and then give a summary and conclusions.

## Site Background and Characterization

The Frio site was chosen for a small scale pilot test of $CO_2$ injection into a brine aquifer specifically to study sequestration issues. The pilot study had goals to safely inject anthropogenic $CO_2$, model the expected flow, sample the fluid in an up-dip observation well and monitor the resulting plume (Hovorka et al. 2006). The selection and characterization of the Frio site, along with stratigraphic figures, has been described in Hovorka et al. (2006) and in this issue (Doughty et al. 2006) and will be summarized here. The injection site was selected in 2003 after characterization of 21 representative saline formations in the onshore United States. The selected aquifer is part of the on-shore Gulf of Mexico Frio formation sandstone, near Houston, TX. The experimental site is in an oil field, where site access, use of an idle well as an observation well, wireline well logs, 3-D seismic, and production data were donated by the operator, Texas American Resources. A new well was drilled for injection about 30 m offset from the existing observation well. The $CO_2$ injection took place over 10 days in October 2004 with about 1600 tons of supercritical $CO_2$ injected into the upper C-sand of the Frio Formation at a depth of 1528.5 - 1534.7 m (5015 to 5030 ft). The downhole pressure was about 150 bars with about 2-3 bar variation during injection (Hovorka et al. 2006). The downhole temperature was about 55°C. At these conditions the $CO_2$ is in a supercritical liquid

105 state with density of 653 kg/m3 and P-wave velocity of 335 m/s (National Institute of
106 Standards and Technology 2006). The injected $CO_2$ is expected to displace the brine
107 with some amount dissolving into the brine.

108 Sandstones of the Oligocene Frio Formation are a potential target for large-volume stor-
109 age because they are part of a thick, regionally extensive sandstone trend that underlies
110 a concentration of industrial sources and power plants along the Gulf Coast of the
111 United States. Detailed characterization was conducted using traditional reservoir as-
112 sessment tools. From this characterization, a numerical reservoir model was created
113 using LBNL's TOUGH2 code (Pruess 2004; Doughty et al. 2006). Geologically con-
114 strained numerical models of injection and monitoring scenarios were prepared and
115 used to optimize the experimental design, well locations and completion, and monitoring
116 tool selection. The upper Frio in the study area is composed of northwest-southeast-
117 elongated fluvial sandstone separated by mudstones and shales that can be correlated
118 over the field but not regionally. The upper Frio "C," "B," and "A" (in lower to upper
119 stratigraphic order) sandstones are part of a trend of fluvial sandstones that were in-
120 creasingly reworked beneath the regionally extensive 60-m-thick (200-ft) shales and
121 mudstones of the overlying Anahuac Formation. The selected injection zone, the upper
122 half of the Frio "C" sandstone, is a 22.8-m (75-ft) upward-fining, fine-grained, poorly in-
123 durated, well-sorted sandstone. The upper part of the "C" sandstone has porosities of
124 30 to 35% and permeabilities of 2,000 to 2,500 md (Hovorka et al. 2006). The top "C"
125 seal is composed of shale, sands, and siltstones that form a minor seal beneath the re-

gional Anahuac Shale but probably a major barrier to vertical flow out of the "C" sandstone.

Structural analysis of the injection interval using logs and 3-D seismic shows that the upper Frio Formation at the test site is within a fault-bounded compartment that is part of a system of radial faults above a nearby salt dome. Dips within the injection compartment are steep. Hand-picked interpretation of the FMI (formation microimager) log by Schlumberger measured dips of 18 degrees to the south at the injection well; interwell correlation measured an average dip of 16 degrees south (Hovorka et al. 2006).

## Seismic Data Acquisition

The data acquisition description is divided into sensors, sources and recording system. For sensors, both the VSP and crosswell surveys used an 80-level 3-component, clamping geophone string, which was supplied by Paulsson Geophysical and was deployed on special tubing. Each of the 80 3-component sensors was independently clamped to the borehole wall, allowing measurement of ground motion (velocity). The sensors were spaced every 7.6 m (25 ft) along the string, so the 80 sensors spanned 610 m (2000 ft) of the borehole. Figure 2 shows the deployment depths of the sensor string. The 3-component sensors allowed optimal measurement of compressional (P) and shear (S) waves, which are orthogonally polarized.

For the crosswell survey, the source was an orbital vibrator, supplied by LBNL The orbital vibrator source is an eccentric mass rotated by an electric motor. The source is wireline operated and fluid coupled to the surrounding formation. The rate of rotation is linearly varied from 0 to 350 Hz and back to stop. Useable energy is acquired above about 70 Hz, giving a 70 to 350 Hz bandwidth. At each source location a clockwise and counter clockwise sweep is recorded. Decomposition of these two sweeps provides two equivalent sources with orthogonal horizontal oscillations (Daley and Cox 2001). Component rotation using P-wave particle motion rotates these two sources into in-line and cross-line equivalents, with in-line being horizontal and in the plane of the two boreholes. This rotation results in a 6-component receiver gather with in-line and cross-line sources for the vertical and two horizontal receiver components. The in-line source generates predominantly P-wave energy while the cross-line source generates predominantly S-wave energy. Consistent generation of both P- and S-waves is a notable feature of the orbital vibrator source.

In the crosswell survey, both the source and receiver spacing was 1.5 m, with the sources spanning 75 m and the sensors spanning 300 m (only the deepest 40 of the 80 sensors were recorded in the crosswell survey). The sensor string was moved five times at 1.5 m intervals to give 1.5 m sensor spacing from the 7.6 m fixed spacing. Five source 'fans' (all source depths for each of 5 sensor string locations) were thus acquired in the crosswell survey. The survey was conducted using the injection well for sensors and the monitoring well for sources. Source and sensor locations were centered on the injection interval.

The VSP used the same 80 level, 3-component geophone string with explosive sources. The explosive shot holes were about 18 m (60 ft.) deep. A single shot with about 3.5 lbs of seismic explosive was recorded for each sensor string location at each shot point. Eight shot points were acquired (Figure 3). The sensors were interleaved to give spacings of 1.5 to 7.5 m (partially because of the needs of the crosswell recording). Smaller sensor spacing has the advantage of increasing spatial sampling and therefore increasing the spatial resolution of subsurface changes. The shotpoints were offset 100 to 1500 m from the sensor well. The locations of the VSP shotpoints were chosen to monitor the estimated $CO_2$ plume location (sites 1-4 in Figure 3) and to provide structural information at the injection site (sites 5-9 in Figure 3). Other sites were planned but not obtained due to permitting issues and local flooding. These sites (one to the Northeast and one to the South, would have allowed imaging to larger offsets (about 500 m) on these azimuths.

## Data Processing and Analysis

The processing of the VSP focused on time lapse change in reflection amplitude of the reservoir horizon. Initial processing included applying time shifts to correct for shot variations (as measured with a surface geophone at each shot point), picking of arrival times at each depth, separation of down-going and up-going (reflected) wavefields, converting reflections to two-way travel time and enhancing the reflected energy signal using frequency-wavenumber filters. A description of these standard VSP processing de-

188 tails is given in Yilmaz (1987). Following these processing steps, an amplitude equaliza-
189 tion was applied using a reflection above the reservoir (the 'control' reflection labeled in
190 Figure 4. This equalization assumes that amplitude changes in a reflector are due to
191 shallow sub-surface changes (such as soil moisture saturation) or changes in the seis-
192 mic source amplitude. Therefore the amplitude change measured in the shallow reflec-
193 tor is subtracted from all the data. Following this equalization, the time-lapse change in
194 the reservoir reflection can be analyzed. The result from source site 1 is shown in Figure
195 4 where we see a clear increase in the reflection strength from the Frio formation. Simi-
196 lar results have been found from the sites 2, 3 and 4. For the VSP geometry, the reflec-
197 tion recorded at each sensor in the well originates at a different reflection point, so we
198 are able to estimate the variation in reflection strength with offset along the azimuth be-
199 tween source and borehole. The VSP reflection change along three azimuths has been
200 spatially mapped using ray tracing (similar to Figure 1a) to give an estimate of the re-
201 flection point location. Comparison of the VSP result with numerical modeling of $CO_2$
202 saturation will be discussed in the following interpretation section.

203 Before tomographic imaging, the travel times for P- and S-waves are determined. Typi-
204 cally the data is sorted into different 'gathers' with a common source depth, common
205 sensor depth, or common source-sensor vertical offset. An example common offset
206 gather of seismograms in Figure 5 shows good quality P- and S-wave direct arrivals,
207 allowing velocity tomography. The travel times were picked manually using the in-line
208 source and in-line sensor for P-wave and the cross-line source and cross-line sensor for
209 S-wave. During the post-injection travel time picking, a large change in waveforms was

observed in the injection zone (seen in Figure 5). This change was interpreted as 'guided waves' generated by a newly formed (and $CO_2$ induced) seismic low-velocity zone. Because guided waves do not follow the ray-theory used in standard tomographic inversion, travel times within the guided-wave zone were not used for inversion of time-lapse changes. Using the remaining picked travel times, tomographic imaging of velocity was performed.

The tomography processing had the following details: limited ray angles (no vertical offsets greater than 100 m), correction for the deviation of the boreholes from vertical (about 3-5 m of lateral offset), a straight ray projection, and a static correction to allow for borehole effects. Importantly, the data were inverted for the change in velocity, rather than inverting for each velocity field and then differencing. In this method the data input to the tomographic inversion is the travel time difference (postinjection time minus preinjection time) for each source-receiver pair. Typically, time-lapse tomography is done by computing two tomographic inversions with each travel time data set (the preinjection and the post injection) separately input to the tomographic inversion. By inverting the difference data, some potential errors (such as source and sensor locations) are minimized or eliminated (Ajo-Franklin et al. 2006; Spetzler 2006). The inversion algorithm is an algebraic reconstruction as described in Peterson et al. (1985). The inversion used a 2 m x 2m pixel size, with plotting interpolated to 0.5 m. The maximum spatial resolution is thus about 2m. Figure 6 shows the tomographic image of P- and S-wave velocity change. The P-wave tomogram shows a clear zone of change in the injection interval with P-wave velocity decreasing over 500 m/s in some pixels. The S-

232 wave tomogram shows only small changes except for a small region near the injection
233 zone where the S-wave velocity is reduced by up to 200 m/s.

234 Figure 7 shows a more detailed view of the P-wave velocity change within the injection
235 zone, along with the well logs indicating $CO_2$ saturation near the boreholes. The well
236 logs are Schlumberger's reservoir saturation tool (RST) (Adolph, et al., 1994). The $CO_2$
237 plume is clearly imaged by the velocity change, and the spatial agreement between the
238 well logs and the tomograms provides mutual corroboration to each of these two inde-
239 pendent measures of $CO_2$. Several attributes of the $CO_2$ induced change in seismic ve-
240 locity can be observed via the tomogram and will be discussed in the interpretation sec-
241 tion.

242 **Interpretation**

243 The injection of $CO_2$ causes a fluid substitution within the pore space. For fluid substitu-
244 tion with no change in matrix properties, a change in P-wave velocity is expected due to
245 the change in bulk modulus (compressibility) with a minimal change in S-wave velocity
246 expected due to the lack of change in shear modulus (which is a property of the rock
247 matrix and not affected by pore fluid). Time-lapse tomographic imaging did map
248 changes in P-wave velocity (over 500 m/s) due to the $CO_2$ plume (Figure 7). The S-
249 wave velocity decrease near the injection well implies that there was some change in
250 rock matrix properties (the shear modulus) in the near well region which was induced by
251 the $CO_2$ injection. Overall, the lack of S-wave change confirms that the observed P-
252 wave change is caused by fluid substitution of $CO_2$ for brine. The small change in

253 pressure (about 3 bars) has a very minimal effect on velocity (about 1-10 m/s) due to
254 the effective stress change. We can therefore interpret the following observations of ve-
255 locity change in terms of $CO_2$ saturation. 1) The velocity change follows the dip of the
256 stratigraphy. This observation is expected for $CO_2$ with buoyancy causing up-dip migra-
257 tion. 2) The velocity change is not homogeneous between the wells, with a larger
258 change, and therefore a larger residual $CO_2$ saturation, in the downdip half of the to-
259 mogram. 3) The velocity change does not reach the actual top of the C-sand, which is
260 in agreement with observed permeability reduction near the top of the sand. 4) The ve-
261 locity change on the right half of the tomogram is somewhat layered with a larger
262 change in the lower part (about 3 m thick) of the plume. This observation implies that
263 the lower part of the plume has higher saturations, presumably due to the presence of a
264 low permeability zone in the center or upper part of the plume.

265 Quantitative estimation of $CO_2$ saturation (the fractional part of the pore space filled
266 with $CO_2$) from the change in seismic velocity is an ultimate goal, and such estimates
267 can be obtained using a rock physics model. For our site, core studies typically used to
268 build a rock physics model have not yet been performed and the unconsolidated sand
269 limited core recovery. Similarly, well log measurement of seismic velocity, which could
270 be closely tied to well log estimates of saturation (the RST log), failed to give useable
271 results for post-injection in the injection zone. Nonetheless, quantitative $CO_2$ saturation
272 estimates from seismic measurements using a rock physics model allow estimation of
273 saturation in the interwell volume. Without site specific calibration we use results from
274 similar high porosity sands such as used in Carcione et al. (2006). The resulting uncer-

275 tainty is difficult to quantify but is probably in the range of 10% in saturation (based on
276 variation with model parameters). We have built a rock physics model using recent work
277 of Hoversten et al. (2003) with data from Carcione et al. (2006) (using the Utsira sand)
278 and a model of fluid mixing proposed by Brie et al. (1995) to estimate the CO saturation
279 from the seismic velocity. The $CO_2$ saturation is shown in Figure 8 where see
280 saturations are estimated at about 20% in the region near the injection well and de-
281 crease to about 10% or less near the monitoring well. The $CO_2$ plume is about 5 m
282 thick with the highest saturations (up to 20%) extending 15 m from the injection well.
283 The lower half of the plume has higher concentrations, implying vertical heterogeneity
284 (variation in permeability or porosity). The vertical variation is at the limit of the tomo-
285 graphic resolution (2 m), so greater detailed interpretation of the vertical heterogeneity is
286 not possible. The saturation values are less than those observed in the RST, although
287 the RST is a near-borehole measurement, not necessarily representative of the interwell
288 region, and the RST had calibration problems for measurements made after the seismic
289 surveys (Hovorka et al. 2006).

290 Interpretation of the VSP is focused on the large change in reflection amplitude and cal-
291 culating this change as a function of offset from the injection well along each azimuth of
292 a VSP source. Because we do not have an estimate of saturation directly from reflec-
293 tion strength, we compare the VSP result to the numerical model estimate of saturation.
294 Figure 9 shows the offset dependent reflection change for a single azimuth with a com-
295 parison to the $CO_2$ saturation estimated at the same offset and azimuth using the
296 TOUGH2 numerical flow model to estimate the spatial distribution of $CO_2$ saturation

297 (Doughty et al. this issue). We see a good qualitative agreement of the plume extent,
298 about 80 m radially. Figure 10 shows this same comparison on three azimuths, North,
299 Northwest and Northeast. We see the agreement is good to the North, moderate to the
300 Northeast and worse to the Northwest. Since the numerical model is laterally and azi-
301 muthally homogeneous (allowing for formation dip), the disagreement indicates lateral
302 heterogeneity imaged by the VSP which is not captured in the model.

303 The large VSP reflection response was somewhat unexpected because of the thinness
304 of the $CO_2$ plume (about 5-7 m thick at 1500 m depth), and uncertainty in the expected
305 velocity change. To verify the VSP result is consistent with the velocity change meas-
306 ured in the crosswell survey, we developed a numerical seismic model. The modeling
307 used a 2-D elastic, finite-difference wave propagation code on a 201 by 652 grid with 5
308 m grid points (1 km by 3.3 km) and a 30 Hz center frequency. The initial 2-D velocity
309 structure was built using horizons mapped from previous surface seismic, velocities
310 measured by the pre-injection VSP, and velocity and density measured by pre-injection
311 well logs. VSP data was generated using this pre-injection model. Two 'post-injection'
312 VSP data sets were then calculated. The 'time-lapse' VSP response was calculated us-
313 ing the same processing as the field data, with the exception of amplitude calibration to
314 a shallower reflection, which is unnecessary for numerical data with no shallow
315 changes.

316 To obtain the post-injection model, we first applied the change in velocity, as mapped by
317 the crosswell tomogram, to the 30 m wide zone between wells. This result un-

318 derestimated the reflection amplitude change measured by the VSP. We then extended
319 the velocity change beyond the wells using a 400 m/s velocity decrease (typical of that
320 seen in the crosswell tomogram) applied to a 4 m thick zone over the horizontal dis-
321 tance predicted to contain $CO_2$ by the numerical flow modeling. This result overesti-
322 mated the reflection amplitude change. These two modeled time-lapse VSP responses
323 are shown in Figure 11, where we see that they bound the field measurement. This re-
324 sult demonstrates that velocity changes, on the order of those imaged by crosswell to-
325 mography, when they are extended beyond the interwell region, are able to generate
326 the large reflection amplitude change observed in the VSP.

327

328 **Conclusions**

329 Sixteen hundred tons of $CO_2$ were injected into a brine aquifer at a depth of 1500 m at
330 the Frio pilot site. Borehole seismic data, both VSP and crosswell, were acquired.
331 Analysis of these time-lapse surveys provided in-situ estimates of the spatial distribution
332 of injected $CO_2$, with high resolution tomographic imaging between injection and moni-
333 toring wells (crosswell), and lower resolution VSP reflection imaging at larger distances,
334 on different azimuths. The crosswell tomogram shows seismic P-wave velocity de-
335 creases up to 500 m/s, while the S-wave velocity shows minimal change. The spatial
336 change in P-wave velocity can be interpreted for details of the $CO_2$ saturation distribu-
337 tion, including buoyant up-dip flow with some layering and less change in velocity on the
338 up-dip half of the tomogram, indicating permeability heterogeneity. Initial development of

a rock physics model allows estimates of $CO_2$ saturation between the wells from the crosswell tomogram. The VSP results, using changes in reflection amplitude from the injection horizon, show a large increase (up to 70%) and show azimuthal variation, also indicating $CO_2$ flow heterogeneity. Numerical modeling of the VSP response uses the crosswell measurements to show that velocity changes seen in the interwell volume can cause the large response in the VSP reflectivity change if the velocity change is extended beyond the wells. It is reasonable to infer that the large reflection response seen in the VSP would allow surface seismic monitoring of similar $CO_2$ plumes, allowing monitoring of small plumes away from boreholes. This result demonstrates that small $CO_2$ plumes (such as those migrating away from a major injection) are detectable in saline aquifers.

**Acknowledgments:**

This work was supported by the GEOSEQ project for the Assistant Secretary for Fossil Energy, Office of Coal and Power Systems through the National Energy Technology Laboratory, of the US Department of Energy, under Contract No.DE-AC02-05CH11231. The CO2 flow modeling results were prepared by Chris Doughty of LBNL. Thanks to Susan Hovorka and Sally Benson for management of the Frio and GEOSEQ projects, respectively, and their support of the geophysics program. Thanks to Don Lippert, Cecil Hoffpauir and Rob Trautz for their important contributions to the data acquisition.

359 Thanks to Bjorn Paulsson of P/GSI . Thanks to the editors and anonymous reviewers for
360 helpful comments and corrections.

361

362 **References:**

363 Adolph B, Stoller C., Brady J., Flaum C., Melcher C,. Roscoe B., Vittachi A. (1994) Satu-
364 ration monitoring with the RST Reservoir Saturation Tool. Oilfield Review 6:29-38.

365 Ajo-Franklin J.B., Urban J, Harris J.M. (2006) Temporal Integration of Seismic
366 Traveltime Tomography. Society of Exploration Geophysicists Annual Meeting, Ex-
367 panded Abstracts 25:2468.

368 Arts R., Elsayed R., Van Der Meer L., Eiken O., Ostmo O., Chadwick A., Kirby G. and
369 Zinszner B. (2002) Estimation of the Mass of Injected $CO_2$ at Sleipner Using Time-
370 Lapse Seismic Data. paper H-16, EAGE 64th Annual Conference.

371 Balch A.H. and Lee M.W., (ed) (1984) Vertical Seismic Profiling: Technique, Applica-
372 tions, and Case Histories. International Human Resources Development Corporation,
373 Boston, MA.

374 Brie A., Pampuri F., Marsala A.F., and Meazza O. (1995) Shear sonic interpretation in
375 gas-bearing sands. SPE Annual Technical Conf., 30595:701-710.

376

377 Carcione J.M., Picotti S., Gei D., Rossi G. (2006) Physics and Seismic Modeling for
378 Monitoring $CO_2$ Storage. Pure and Applied Geophysics 163:175 – 207 DOI
379 10.1007/s00024-005-0002-1.
380
381 Daley T.M. and Cox D. (2001) Orbital vibrator seismic source for simultaneous P- and
382 S-wave crosswell acquisition. Geophysics 66:1471-1480.
383
384 Gritto R., T.M. Daley and L.R. Myer (2004) Joint cross-well and single-well seismic stud-
385 ies at Lost Hills, California. Geophysical Prospecting 52:323-339

386 Hardage B.A. (2000) Vertical Seismic Profiling: Principles, Handbook of Geophysical
387 Exploration: Seismic Exploration, 14, Elsevier.

388 Harris J.M., Nolen-Hoeksema R.C., Langan R.T., Van Schaack M., Lazaratos S.K.,
389 Rector J.W. (1995) High-resolution crosswell imaging of a west Texas carbonate reser-
390 voir: Part1-Project summary and interpretation. Geophysics 60:667-681.

391 Hoversten G., M., Gritto R., Washbourne J., Daley T. M, (2003) Pressure and Fluid
392 Saturation Prediction in a Multicomponent Reservoir, using Combined Seismic and
393 Electromagnetic Imaging. Geophysics 68:1580-1591.
394
395 Hovorka S.D., Benson S.M., Doughty C., Friefeld B.M., Sakurai S., Daley T.M. (2006)
396 Measuring permanence of CO2 storage in saline formations: the Frio experiment. Envi-
397 ronmental Geosciences 13:1-17 DOI:10.1306/eg.11210505011

Lazaratos S.K., and Marion B.P. (1997) Crosswell seismic imaging of reservoir changes caused by CO2 injection. The Leading Edge 16:1300-1306.

Majer E.L., Daley T.M., Korneev V., Cox D., Peterson J.E. (2006) Cost-effective imaging of CO2 injection with borehole seismic methods. The Leading Edge, 25, p1290.

National Institute of Standards and Technology (2006), Thermophysical Properties of Carbon Dioxide. http://webbook.nist.gov/cgi/fluid.cgi?ID=C124389&Action=Page Cited Nov 17, 2006.

Pacala S., and Socolow R. (2004) Stabilization Wedges: Solving the Climate Problem for the Next 50 Years with Current Technologies. Science 305:968-972.

Peterson, J.E. Paulsson B.N. and McEvilly T.V. (1985) Applications of algebraic reconstruction techniques to crosshole seismic data. Geophysics 50:1566-1580.

Pruess K. (2004) The TOUGH Codes - A Family of Simulation Tools for Multiphase Flow and Transport Processes in Permeable Media. Vadose Zone Journal 3:738-746.

Spetzler J., (2006) Time-Lapse Seismic Crosswell Monitoring of Steam Injection in Tar Sand, Society of Exploration Geophysicists Annual Meeting, Expanded Abstracts v25, p3120.

Spetzler J., Xue Z., Saito H., Nobuoka D., Hiroyuki A., Nishizawa O. (2006) Time-Lapse Seismic Crosswell Monitoring of Co2 injected in an Onshore Sandstone Aquifer. Society of Exploration Geophysicists Annual Meeting, Expanded Abstracts 25:3285.

418 Yilmaz O. (1981) Seismic Data Processing. Investigations in Geophysics no. 2, Society
419 of Explorations Geophysicists.

420

421 Xue Z., Tanase D., Saito H., Nobuoka D., Watanabe J (2005) Time-lapse crosswell
422 seismic tomography and well logging to monitor the injected CO2 in an onshore aquifer.
423 Nagaoka, Japan, Society of Exploration Geophysicists Annual Meeting, Expanded Ab-
424 stracts 24:1433.

425

Figure Captions:

Figure 1a (left) Schematic of VSP data acquisition with direct raypaths (yellow), reflected raypaths (blue), and boreholes (yellow and purple vertical lines)

1b) (right) Schematic of crosswell acquisition with sensors (green) and sources (red) in separate boreholes (yellow and purple) with raypaths in yellow.

Figure 2. Sensor string deployment depths with each line segment representing one deployment. FFID is the field file identification number. For the crosswell deployments only the bottom half of the sensors were recorded.

Figure 3. VSP shot point locations along with the two wells (in light blue).

Figure 4. VSP reflection amplitude comparison. A large increase in amplitude is observed for the Frio reflection. The control reflection is the one used for amplitude normalization between surveys.

Figure 5. Comparison of zero-offset gathers from the crosswell survey. A decrease in travel time within the injection zone can be observed.

Figure 6. Tomographic image of P-wave velocity change (left) and S-wave velocity change (right) from the crosswell survey.

Figure 7. Detailed view of the injection region of the P-wave tomogram along with RST logs for each well. The RST log had multiple runs with the change shown in yellow.

Figure 8. CO2 saturation estimated from the P-wave velocity change using a rock physics model.

Figure 9. VSP reflection amplitude change compared with CO2 saturation estimated by flow modeling, as a function of offset from the injection well on the Northern azimuth.

Figure 10 VSP reflection amplitude change compared with CO2 saturation estimated by flow modeling, as a function of offset from the injection well on three azimuths.

Figure 11. Numerical modeling of VSP reflection amplitude change compared to field data. The model using the predicted plume extent extendes the velocity change over more than 130 m laterally, While the variable change model only had velocity change between the wells (about 30 m).

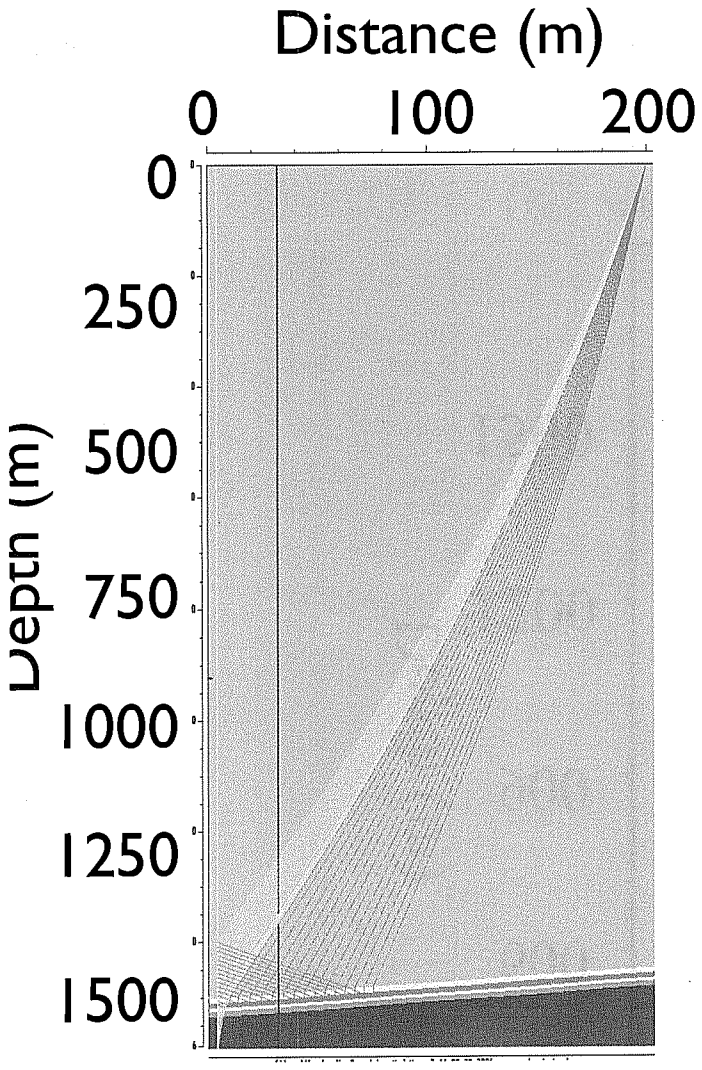


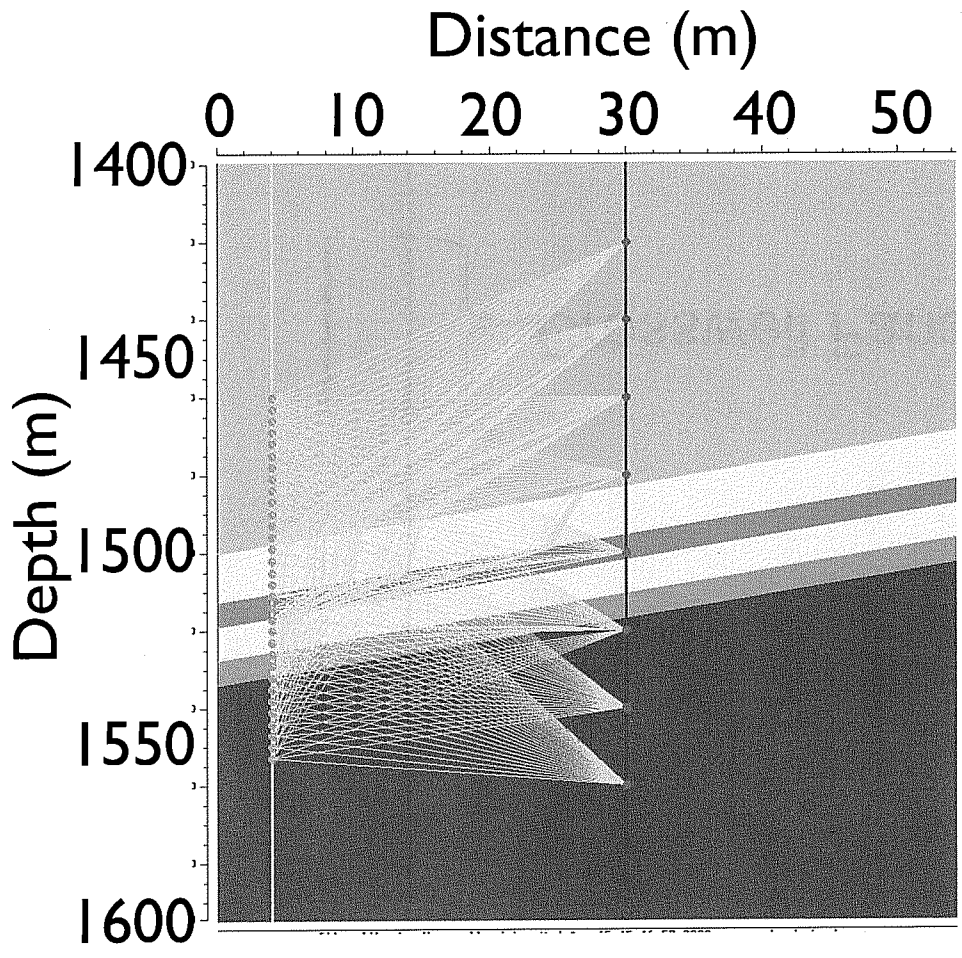


Figure 1a (left) Schematic of VSP data acquisition with direct raypaths (yellow), reflected raypaths (blue), and boreholes (yellow and purple vertical lines)
1b) (right) Schematic of crosswell acquisition with sensors (green) and sources (red) in separate boreholes (yellow and purple) with raypaths in yellow.

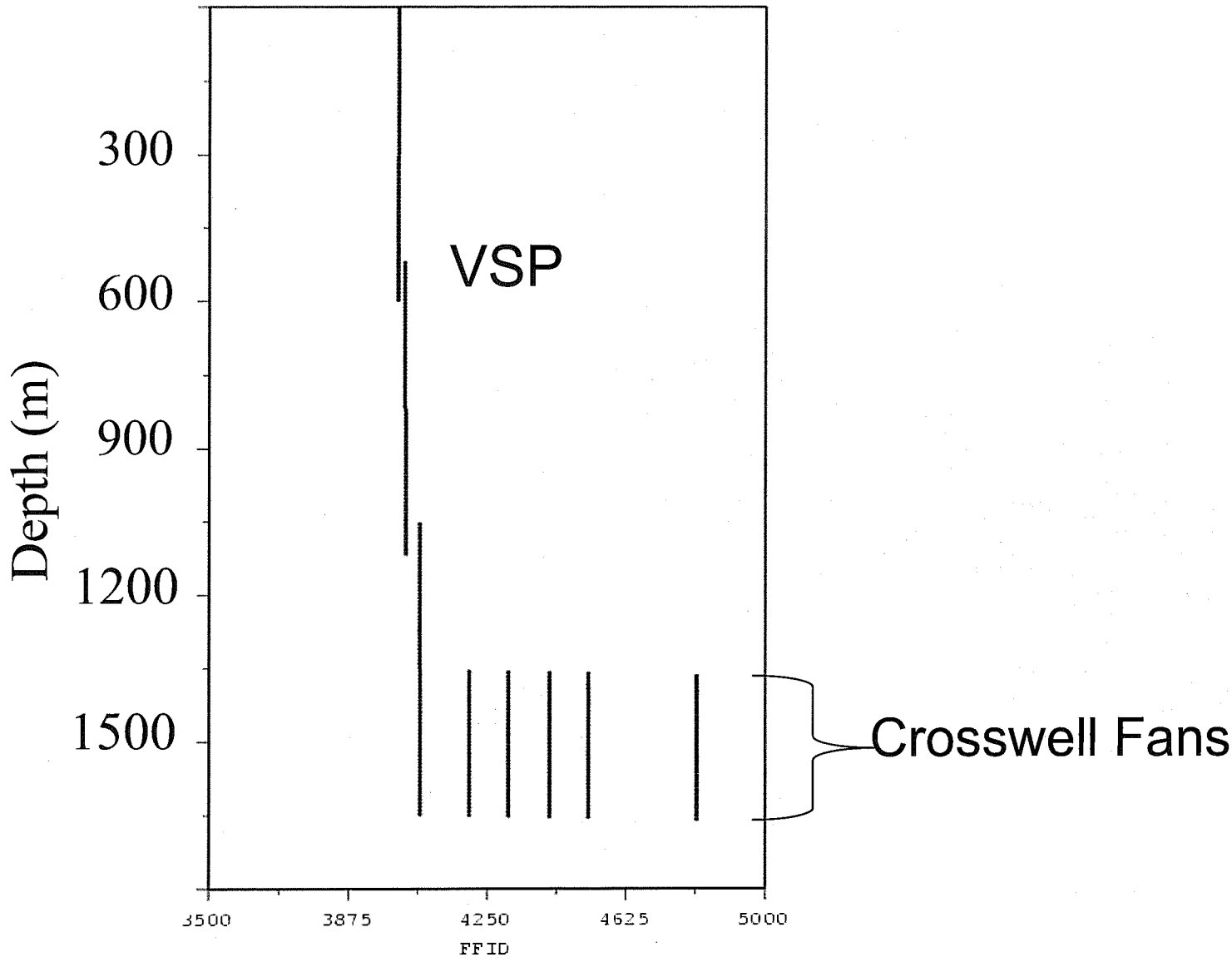


Figure 2. Sensor string deployment depths with each line segment representing one deployment. FFID is the field file identification number. For the crosswell deployments only the bottom half of the

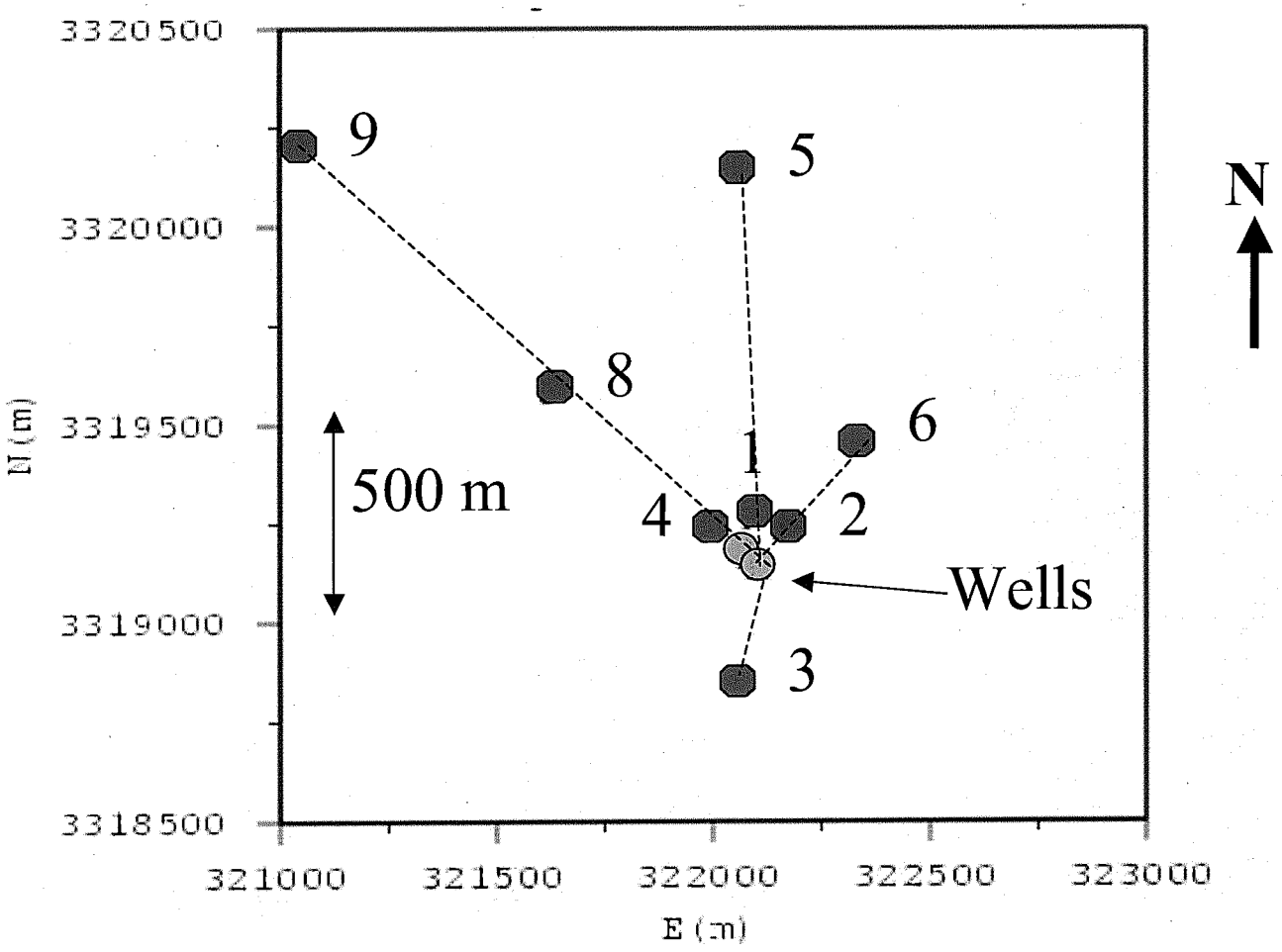


Figure 3. VSP shot point locations along with the two wells (in light blue).

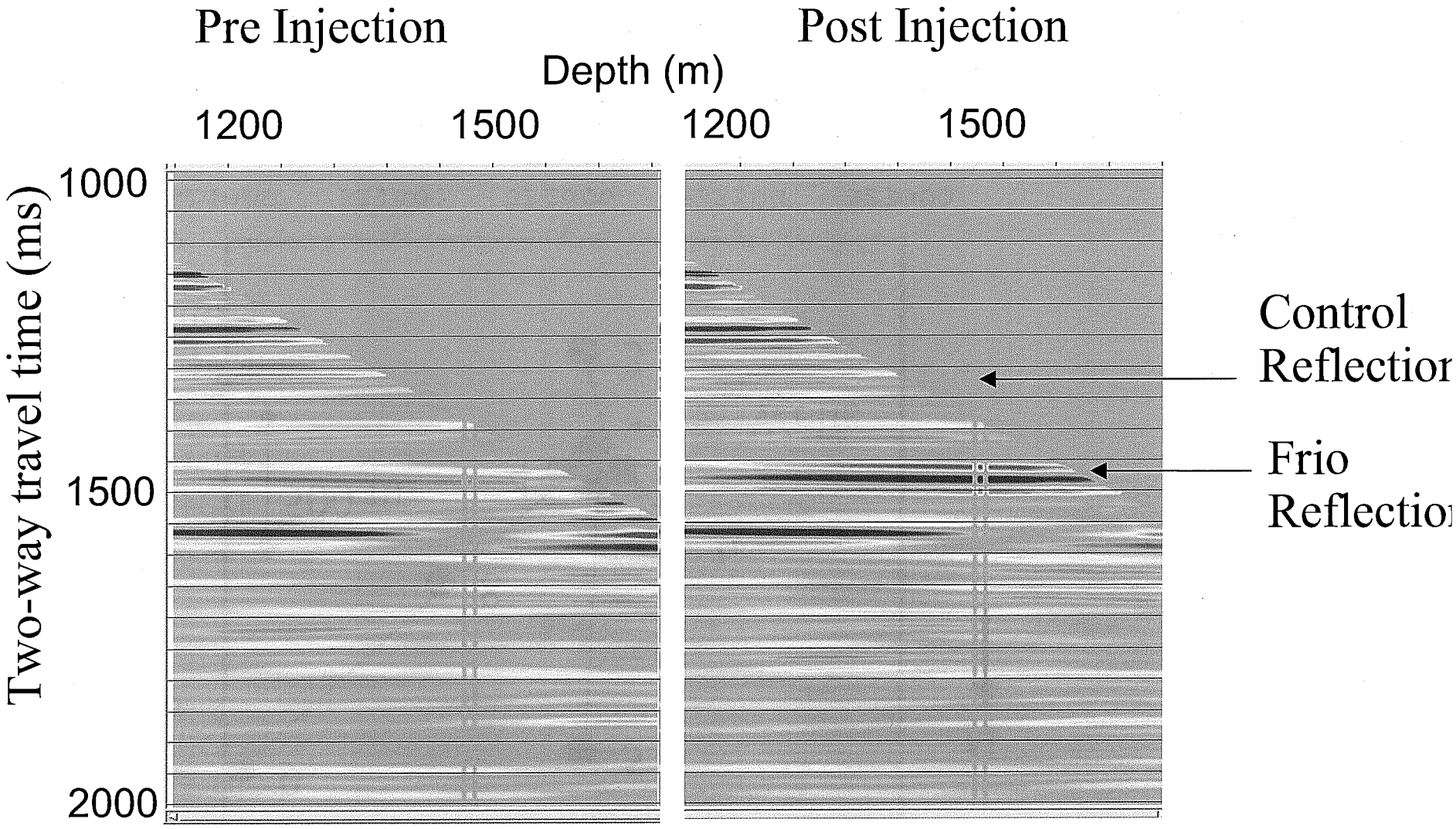


Figure 4. VSP reflection amplitude comparison. A large increase in amplitude is observed for the Frio reflection. The control reflection is the one used for amplitude normalization between surveys.

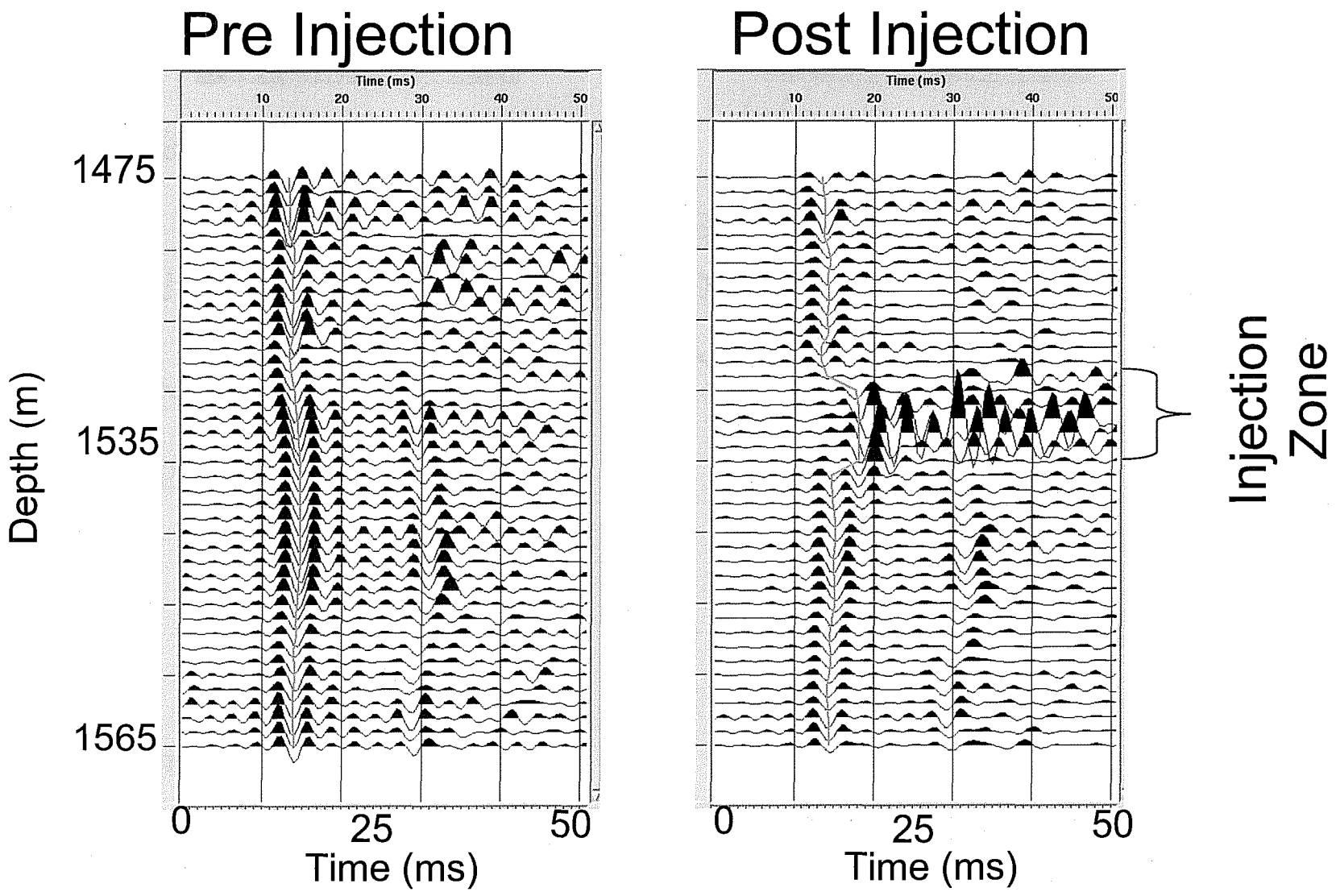


Figure 5. Comparison of zero-offset gathers from the crosswell survey. A decrease in travel time within the injection zone can be observed.

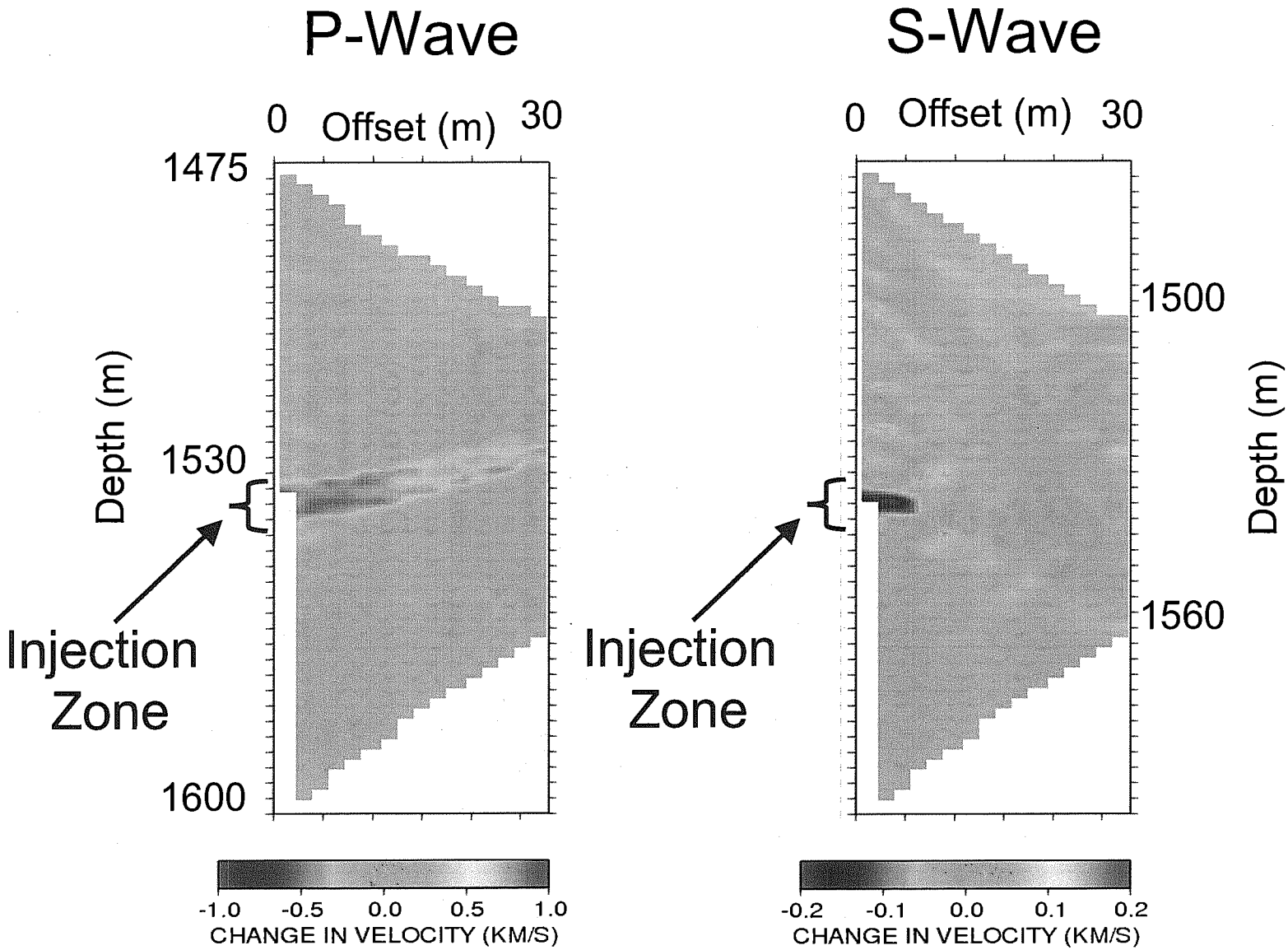


Figure 6. Tomographic image of P-wave velocity change (left) and S-wave velocity change (right) from the crosswell survey.

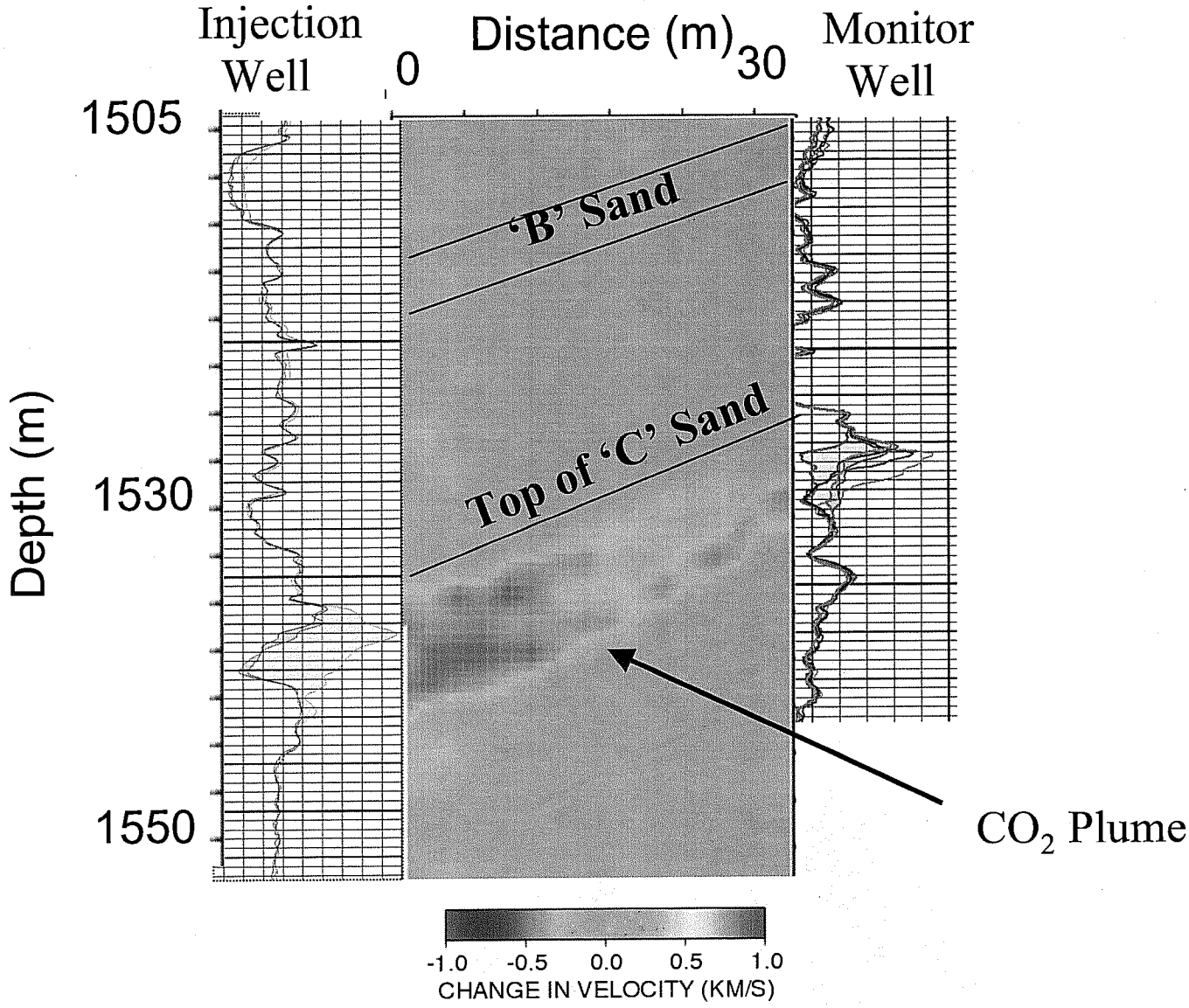


Figure 7. Detailed view of the injection region of the P-wave tomogram along with RST logs for each well. The RST log had multiple runs with the change shown in yellow.

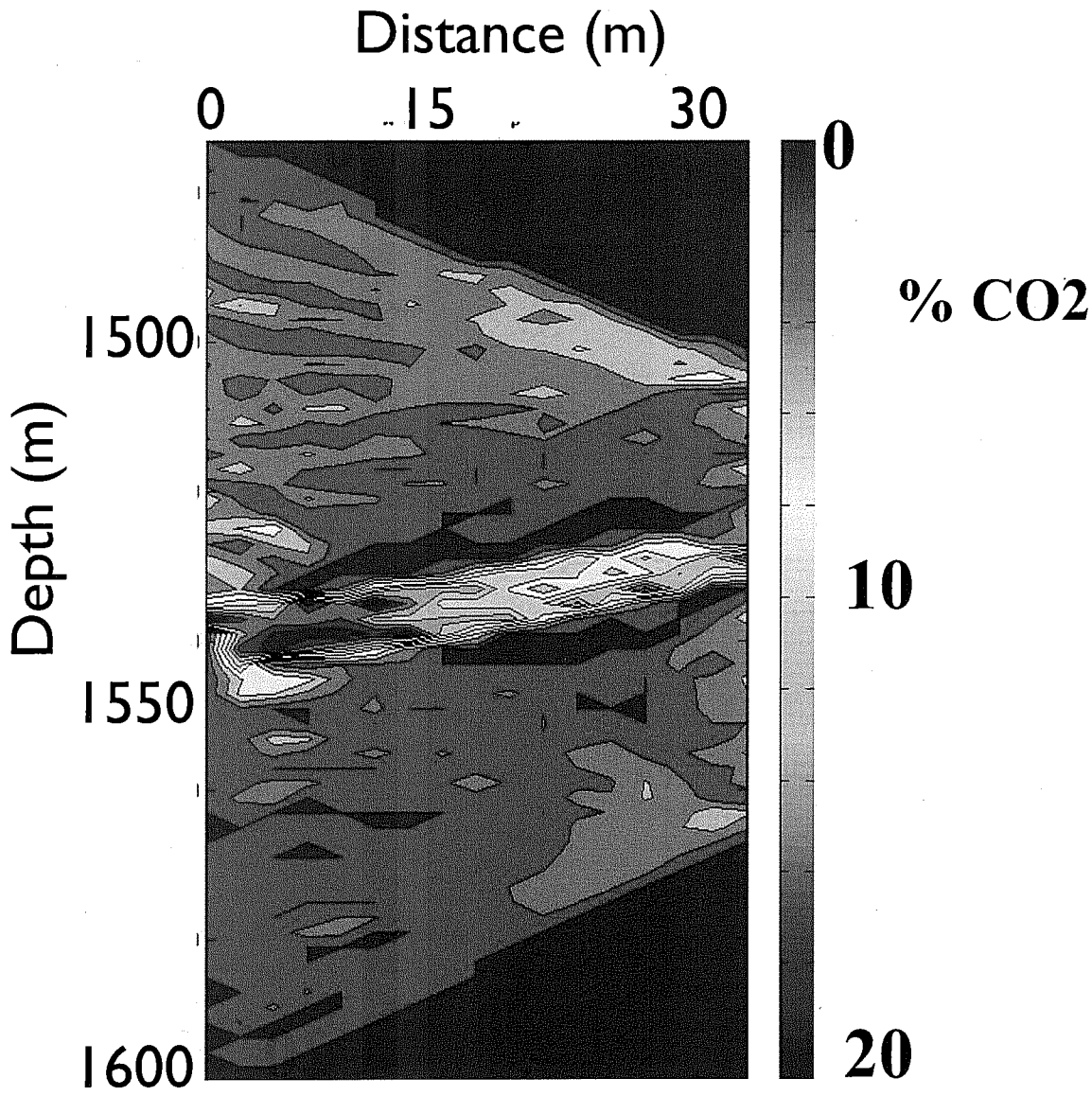


Figure 8. CO2 saturation estimated from the P-wave velocity change using a rock physics model.

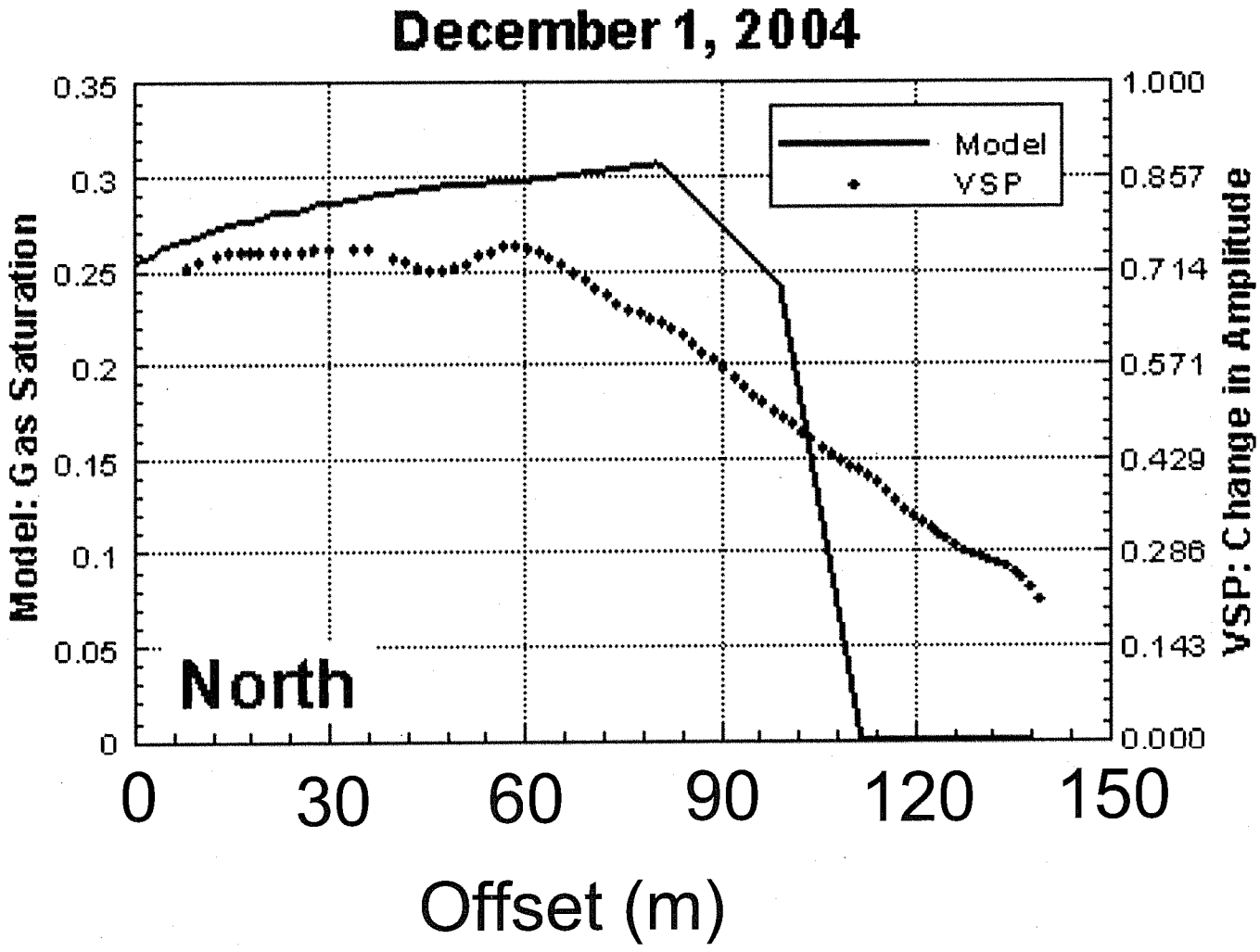


Figure 9. VSP reflection amplitude change compared with CO2 saturation estimated by flow modeling, as a function of offset from the injection well on the Northern azimuth.

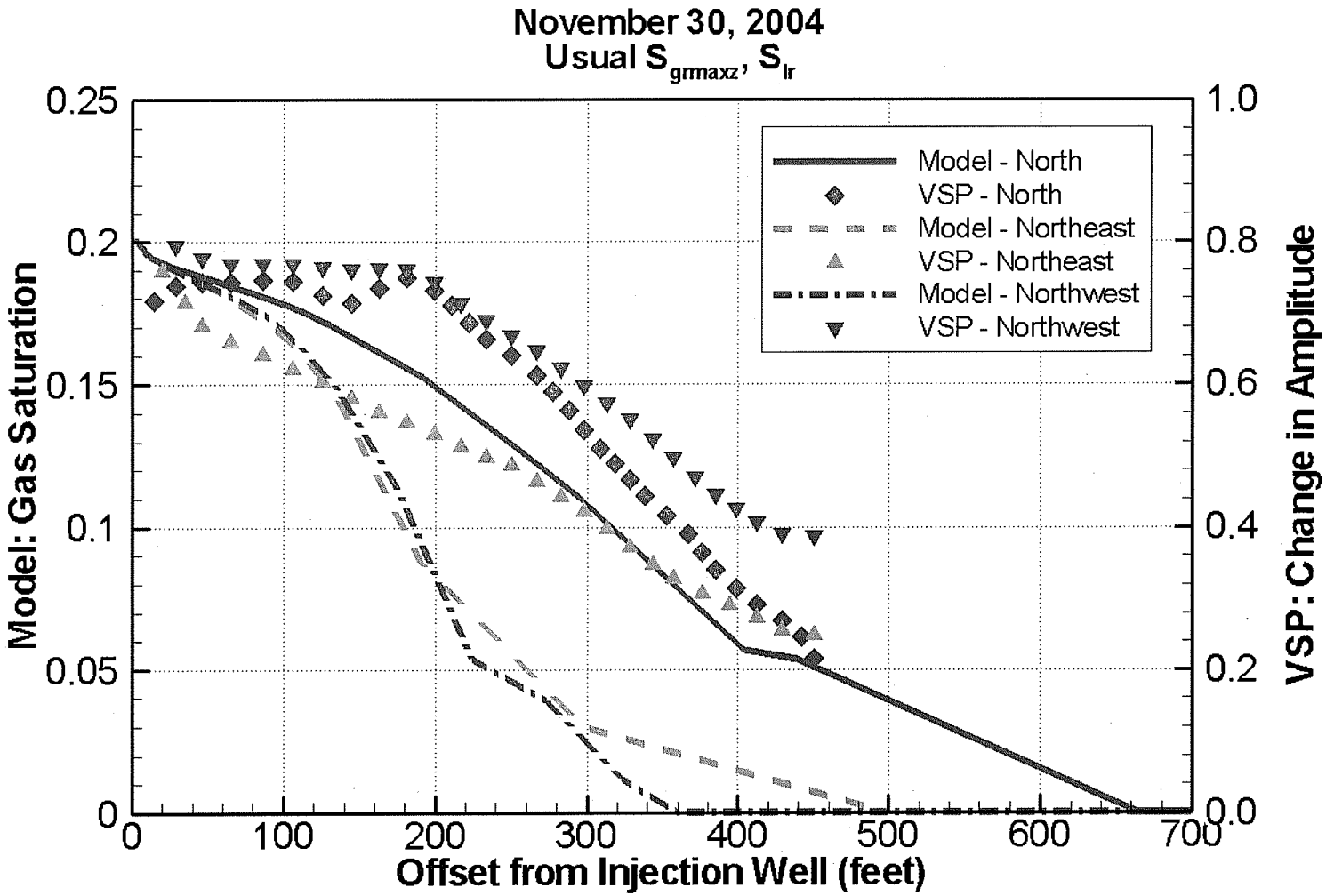


Figure 10 VSP reflection amplitude change compared with CO2 saturation estimated by flow modeling, as a function of offset from the injection well on three azimuths.

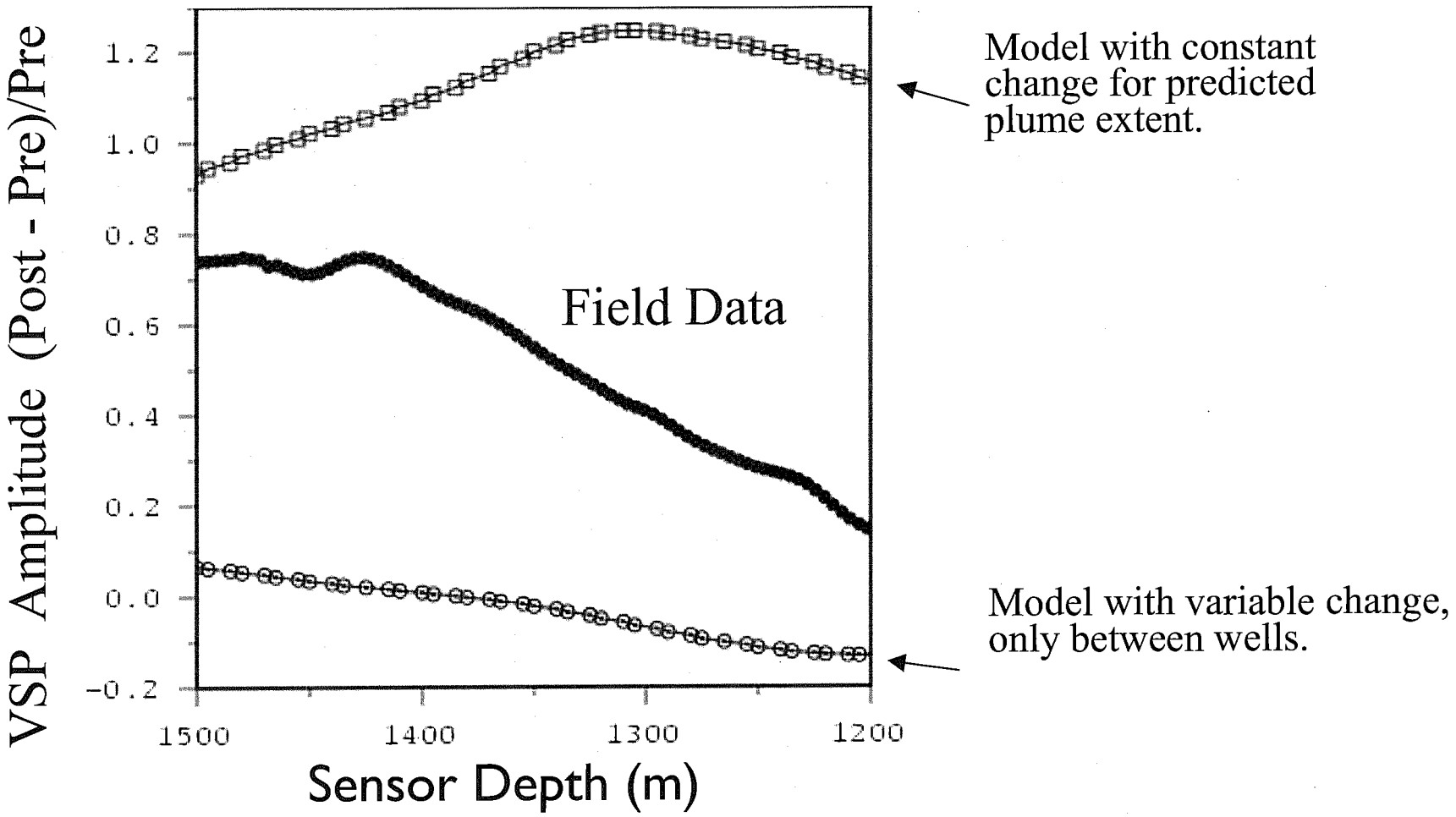


Figure 11. Numerical modeling of VSP reflection amplitude change compared to field data. The model using the predicted plume extent extendes the velocity change over more than 130 m laterally, While the variable change model only had velocity change between the wells (about 30 m).